Upper Limit on the Chiral Magnetic Effect in Isobar Collisions at the Relativistic Heavy-Ion Collider

The STAR Collaboration
(Dated: October 23, 2023)

The chiral magnetic effect (CME) is a phenomenon that arises from the QCD anomaly in the presence of an external magnetic field. The experimental search for its evidence has been one of the key goals of the physics program of the Relativistic Heavy-Ion Collider. The STAR collaboration has previously presented the results of a blind analysis of isobar collisions ($^{96}_{44}\mathrm{Ru}+^{96}_{44}\mathrm{Ru}$, $^{96}_{40}\mathrm{Zr}+^{96}_{40}\mathrm{Zr}$) in the search for the CME. The isobar ratio (Y) of CME-sensitive observable, charge separation scaled by elliptic anisotropy, is close to but systematically larger than the inverse multiplicity ratio, the naive background baseline. This indicates the potential existence of a CME signal and the presence of remaining nonflow background due to two- and three-particle correlations which are different between the isobars. In this post-blind analysis, we estimate the contributions from those nonflow correlations as a background baseline to Y, utilizing the isobar data as well as HIJING simulations. This baseline is found consistent with the isobar ratio measurement, and an upper limit of 10% at 95% confidence level is extracted for the CME fraction in the charge separation measurement in isobar collisions at $\sqrt{s_{\mathrm{NN}}}=200$ GeV.

Introduction. The chiral magnetic effect (CME) refers to an electric current (charge separation of produced particles) along the strong magnetic field produced in relativistic heavy-ion collisions due to chirality-imbalanced, parity and charge-parity odd metastable domains [1]. The formation of such domains has been predicted by quantum chromodynamics (QCD) to occur at high temperatures in those collisions because of vacuum fluctuations [2–5] and may be pertinent to the matter-antimatter asymmetry of our universe [6].

To measure charge separation, three-point correlators,

$$\begin{aligned}\gamma_{\alpha\beta} =&\langle\cos(\phi_\alpha+\phi_\beta-2\psi_{\mathrm{RP}})\rangle\\ \Delta\gamma =&\gamma_{\mathrm{OS}}-\gamma_{\mathrm{SS}},\end{aligned} \tag{1}$$

are used [7]. The terms $\phi_{\alpha,\beta}$ represent the azimuthal angles (in the plane perpendicular to the beam axis) of particles of interest (α,β), which are of either opposite sign (OS) or same sign (SS) in electric charge. The average $\langle\cdots\rangle$ is taken over particle pairs and events. The term ψ_{RP} is the azimuthal angle of the reaction plane, defined by the beam and impact parameter directions. While charge-independent backgrounds are canceled in $\Delta\gamma$, backgrounds remain from two-particle (2p) correlations coupled with the elliptic flow of those correlation sources, such as resonances and jets [7–10]. These backgrounds dominate charge separation measurements at the Relativistic Heavy-Ion Collider (RHIC) [11–19] and the Large Hadron Collider (LHC) [20–23].

To eliminate backgrounds, isobar $^{96}_{44}\mathrm{Ru}+^{96}_{44}\mathrm{Ru}$ and $^{96}_{40}\mathrm{Zr}+^{96}_{40}\mathrm{Zr}$ collisions at nucleon-nucleon center-of-mass energy of $\sqrt{s_{\mathrm{NN}}}=200$ GeV were conducted in a single year data collection (2018) by the Solenoid Tracker At RHIC (STAR) [24]. Due to the identical mass number, backgrounds were expected to be equal in those collision systems, whereas an appreciable CME signal difference would exist because of the different atomic numbers responsible for the magnetic field [25, 26]. However, contrary to expectations, the isobar data [24] show that the two systems have different background contributions: the two isobars differ by up to a few percent in the produced charged particle multiplicities (4.4%) and the elliptic flows (1.4%). These differences are consistent with energy density functional calculations of the nuclear structures, resulting in a smaller Ru nucleus than the Zr nucleus [27–29]. Although the $\Delta\gamma/v_2$ was constructed to account for the elliptic flow (parameterized by v_2) difference, the isobar (Ru+Ru/Zr+Zr) ratio of the $\Delta\gamma/v_2$ measurements, $Y\equiv\frac{(\Delta\gamma/v_2^*)^{\mathrm{Ru}}}{(\Delta\gamma/v_2^*)^{\mathrm{Zr}}}$, was smaller than unity due to the multiplicity difference that was not considered in the blind analysis [24].

If the number of correlation sources is proportional to multiplicity, then Y would be equal to the isobar ratio of the inverse multiplicity ($1/N$) for a pure flow-driven background scenario. A quantitative comparison shows that Y is slightly larger than the $1/N$ ratio [24], indicating the potential presence of a CME signal [30]. However, the measurement of the relative pair excess $r=(N_{\mathrm{OS}}-N_{\mathrm{SS}})/N_{\mathrm{OS}}$ [24] indicates a violation of such proportionality, which is one indication that this naive baseline is not strictly correct. In order to search for any residual signals of CME, a more rigorous evaluation of the background baseline is necessary, which is the main goal of this Letter. Further details of the background assessment analysis can be found in the long companion paper [31].

Refined baseline. In off-center heavy-ion collisions, the azimuthal distribution of final-state particles is anisotropic because of the anisotropic expansion of the collision fireball [32]. The second azimuthal harmonic, elliptic flow, is used to reconstruct ψ_{RP}, the accuracy of which is corrected by a resolution factor [33]. Equivalent to Eq. (1), but more directly, γ can also be calculated using the three-particle (3p) correlator [12], $C_{3,\alpha\beta}=\langle\cos(\phi_\alpha+\phi_\beta-2\phi_c)\rangle$ and $\gamma_{\alpha\beta}=C_{3,\alpha\beta}/v_2$, where v_2 is

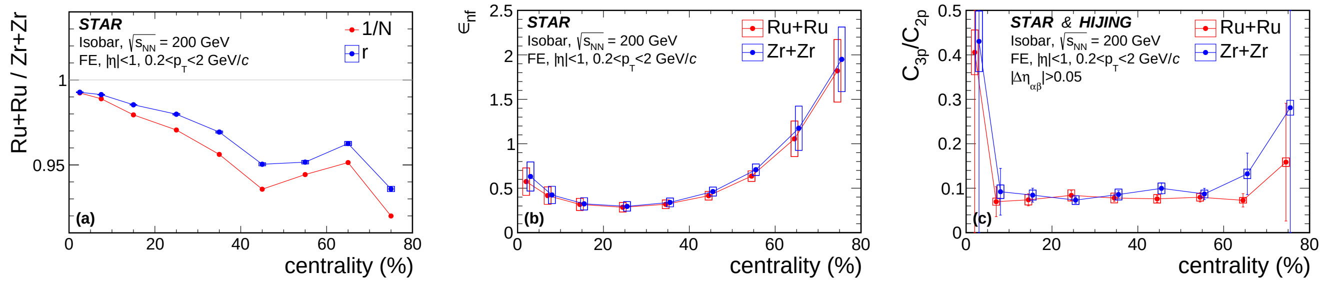

FIG. 1. (a) isobar ratio of $r \equiv (N_{\rm OS} - N_{\rm SS})/N_{\rm OS}$ and inverse multiplicity $(1/N)$; (b) nonflow v_2 contamination $\epsilon_{\rm nf}$; (c) $C_{\rm 3p}/C_{\rm 2p}$ where $C_{\rm 3p}$ is estimated using HIJING and $C_{\rm 2p}$ is from ZDC measurement in [24]. All quantities in these plots use Group-3 full-event (FE) cuts from [24]; other cuts give similar results.

the elliptic flow of particles of type c, which are usually taken as all charged hadrons in a given detector acceptance. The background contribution to $\Delta\gamma/v_2$ from intrinsic 2p and 3p correlation can be expressed [34] as

$$\frac{\Delta\gamma_{\rm bkgd}}{v_2^*} = \frac{C_{\rm 2p}}{N}\frac{v_2^2}{v_2^{*2}} + \frac{C_{\rm 3p}}{N}\frac{1}{N_c v_2^{*2}} = \frac{C_{\rm 2p}}{N}\frac{1+\frac{C_{\rm 3p}/C_{\rm 2p}}{Nv_2^2}}{1+\epsilon_{\rm nf}}\,, \tag{2}$$

where

$$\frac{C_{\rm 2p}}{N} = \frac{N_{\rm 2p}}{N_{\rm OS}}\left(C_{\rm 2p,OS}\frac{v_{2,\rm 2p}}{v_2} - \frac{\gamma_{\rm SS}}{v_2}\right), \tag{3}$$

$$\frac{C_{\rm 3p}}{N} = \frac{N_{\rm 3p,OS}}{N_{\rm OS}}C_{\rm 3p,OS} - \frac{N_{\rm 3p,SS}}{N_{\rm SS}}C_{\rm 3p,SS}\,. \tag{4}$$

The notation $C_{\rm 2p,OS} = \langle\cos(\phi_\alpha+\phi_\beta-2\phi_{\rm 2p})\rangle_{\rm 2p,OS}$ refers to those correlated background pairs only, where $\phi_{\rm 2p}$ is the azimuth of the pair, $N_{\rm OS}$ and $N_{\rm SS}$ are OS and SS pair multiplicities, and $N_{\rm 2p} \equiv N_{\rm OS} - N_{\rm SS}$. Similarly, $C_{\rm 3p,OS} = \langle\cos(\phi_\alpha+\phi_\beta-2\phi_c)\rangle_{\rm 3p,OS}$ and $C_{\rm 3p,SS}$ refer to those correlated background triplets only, where $N_{\rm 3p,OS}$ and $N_{\rm 3p,SS}$ are their triplet multiplicities. N is the multiplicity of particles of interest (POI), and N_c is that of particle c (in this analysis $N = N_c$). The v_2 and $v_{2,\rm 2p}$ refer to the *true* elliptic flow of POIs and those correlated 2p sources, respectively. The quantity v_2^* refers to the measured elliptic flow, which contains *nonflow*–correlations unrelated to the global collision geometry. The equation,

$$\epsilon_{\rm nf} = (v_2^*/v_2)^2 - 1\,, \tag{5}$$

quantifies the relative nonflow contamination.

The isobar ratio can then be decomposed into

$$Y_{\rm bkgd} \equiv \frac{(\Delta\gamma_{\rm bkgd}/v_2^*)^{\rm Ru}}{(\Delta\gamma_{\rm bkgd}/v_2^*)^{\rm Zr}} \approx 1 + \frac{\delta(C_{\rm 2p}/N)}{C_{\rm 2p}/N} - \frac{\delta\epsilon_{\rm nf}}{1+\epsilon_{\rm nf}} + \frac{1}{1+\frac{Nv_2^2}{C_{\rm 3p}/C_{\rm 2p}}}\left(\frac{\delta C_{\rm 3p}}{C_{\rm 3p}} - \frac{\delta C_{\rm 2p}}{C_{\rm 2p}} - \frac{\delta N}{N} - \frac{\delta v_2^2}{v_2^2}\right), \tag{6}$$

where $\delta X \equiv X^{\rm Ru} - X^{\rm Zr}$ for any $X = C_{\rm 3p}$, $C_{\rm 2p}$, etc., while all other quantities without "δ" refer to those in Zr+Zr. Equation (6) suggests categorizing the nonflow contributions to the background into three ingredients: (1) $\delta(C_{\rm 2p}/N)/(C_{\rm 2p}/N)$ which characterizes the relative difference of flowing clusters between the two isobars; (2) differences that arise from using v_2^* rather than true flow in the calculation of $\Delta\gamma$, characterized by $\epsilon_{\rm nf}$; (3) differences in the relative amounts (or character) of three particle clusters between the isobars. In the next section we will discuss each of these three in turn. We note that global spin alignment of ρ mesons can introduce an additional background to the CME [35]. Effect of such a background on isobar measurements needs to be assessed in future studies.

Analysis. The isobar blind analysis [24] presented seven different measurements of $\Delta\gamma/v_2$ from four groups; four of these measurements utilized the 2p cumulants for the v_2 measurement and the 3p correlators for $\Delta\gamma$. The other three employed the event-plane method, which is similar, but the nonflow effects are more complicated to assess. We focus on the four cumulant measurements with their corresponding analysis cuts with subtle differences. The same event selections and track quality cuts are used as those in the isobar blind analysis [24].

The background baseline estimate of Eq. (6) requires three ingredients. The first ingredient $\delta(C_{\rm 2p}/N)/(C_{\rm 2p}/N)$, which is related to 2p nonflow, is primarily determined by $N_{\rm 2p}/N_{\rm OS}$, since $(C_{\rm 2p,OS}v_{2,\rm 2p} - \gamma_{\rm SS})/v_2$ (dominated by the first term) should be highly

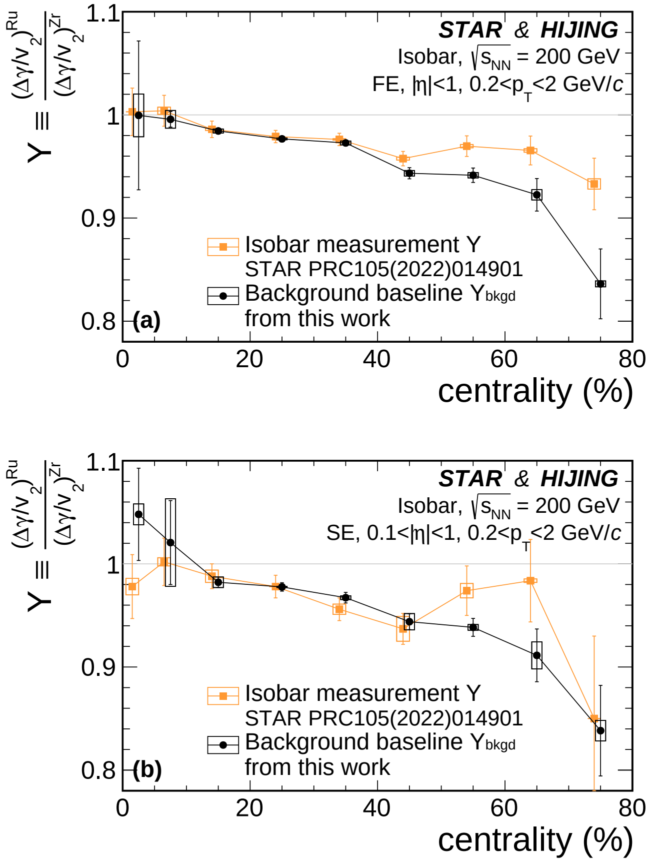

FIG. 2. Estimate of background baseline $Y_{\rm bkgd}$ for the isobar measurement $Y = \frac{(\Delta\gamma/v_2)^{\rm Ru}}{(\Delta\gamma/v_2)^{\rm Zr}}$ as a function of centrality for (a) the full-event (FE) analysis of Group-3 and (b) the subevent (SE) analysis of Group-2; others are similar.

similar between the isobar systems. We analyze $r \equiv N_{\rm 2p}/N_{\rm OS}$ of identified pions as done in [24]. Since $(C_{\rm 2p,OS}v_{2,\rm 2p} - \gamma_{\rm SS})/v_2$ likely depends on the pair invariant mass ($m_{\rm inv}$), we take the average $\delta r/r$ over the entire $m_{\rm inv}$ range as the default and assess systematic uncertainties by considering the range $m_{\rm inv} < 1$ GeV/c^2 [31]. Figure 1(a) shows the isobar ratio of r as a function of centrality from the full-event analysis. For comparison, the efficiency-corrected inverse POI multiplicity ratio is also shown. The $\delta(C_{\rm 2p}/N)/(C_{\rm 2p}/N) \approx \delta r/r$ value averaged over 20–50% centrality is on the order of -3% [31]. Consequently, the baseline $Y_{\rm bkgd}$ is altered by this amount from unity.

The second ingredient is the nonflow contamination in the v_2^* measurement. To estimate it, we fit the acceptance-corrected $(\Delta\eta, \Delta\phi)$ 2p correlations for SS pairs from the full-event analysis by $\Delta\eta$-independent flow harmonics plus $\Delta\eta$- and $\Delta\phi$-dependent nonflow contributions [31]. The true flow is assumed to be the same for the OS and SS pairs. The fitted v_2 parameter, as an estimate of true v_2, is approximately 5.5% in the 20–50% centrality range, with a relative difference of approximately 2.2% between Ru+Ru and Zr+Zr collisions [31]. With the fitted v_2, the $\epsilon_{\rm nf}$ can be readily calculated from the v_2^* cumulant measurements [24]. The v_2^* measurements used slightly different $\Delta\eta$ gaps and various methods; the full-event v_2^* from Group-2 applied Gaussian fits in $\Delta\eta$ to reduce short-range nonflow contributions [24]. The $\epsilon_{\rm nf}$ value ranges from 18–34% depending on the analysis methods. The systematic uncertainties on $\epsilon_{\rm nf}$ are estimated by applying a different acceptance-correction method for the $(\Delta\eta, \Delta\phi)$ correlations [31], by comparing the calculated v_2^* from this analysis to those measured in [24], and by the observed 3% flow decorrelation over one unit of pseudorapidity based on a separate study from STAR [36]. The last source, common to both isobars, cancels in $\delta\epsilon_{\rm nf}/(1+\epsilon_{\rm nf})$. Figure 1(b) shows $\epsilon_{\rm nf}$ as a function of centrality from the full-event analysis without an η gap. The $\epsilon_{\rm nf}$ value is smaller in Ru+Ru than in Zr+Zr because of the larger multiplicity dilution in the former; the actual nonflow correlation strength after factoring out the multiplicity difference is larger in Ru+Ru than Zr+Zr by approximately 2%. The $-\delta\epsilon_{\rm nf}/(1+\epsilon_{\rm nf})$ value ranges from 0.6% to 1.5%, being smaller for subevent than for full event [31]. This correction increases $Y_{\rm bkgd}$ by this amount.

The third ingredient is the genuine 3p correlation background. As 3p correlation measurements are challenging to measure due to the substantial combinatorial background in heavy-ion collisions, we resort to HIJING (Heavy Ion Jet INteraction Generator) simulations [37, 38]. Since HIJING does not have flow, the inclusive 3p correlation from HIJING is in entirety the $C_{\rm 3p}$, purely from the correlated triplets. The $C_{\rm 3p}$ from HIJING simulations with jet quenching is taken as default, and that from quenching-off simulations (about 20% higher) is considered as one side of the maximum systematic uncertainty (i.e., the quoted uncertainty is $1/\sqrt{3}$ of that) with the other side treated symmetrically [31]. The systematic uncertainties on $\delta C_{\rm 3p}/C_{\rm 3p}$ are assessed similarly. HIJING is found to give an adequate description of the peripheral data [31], suggesting that HIJING is a reliable estimator for $C_{\rm 3p}$.

The effect of 3p correlation on $Y_{\rm bkgd}$ also depends on $C_{\rm 2p}$. The $C_{\rm 2p}$ value can be estimated directly from the corresponding zero-degree calorimeter (ZDC) measurements of $N\Delta\gamma/v_2$ because it largely eliminates v_2 nonflow and 3p correlations due to the large η gap between the ZDC and TPC. A one-sided -5% systematic uncertainty is assigned to account for any possibly small CME signal contained in the measurement. No ZDC measurement is available in [24] corresponding to the Group-2 subevent analysis cuts, so it is analyzed in this work to estimate $C_{\rm 2p}$. Figure 1(c) shows $C_{\rm 3p}/C_{\rm 2p}$ as a function of centrality for the full-event analysis from approximately 7.0 billion HIJING events for each isobar. The relative strength of 3p to 2p correlations is on the order of 10%.

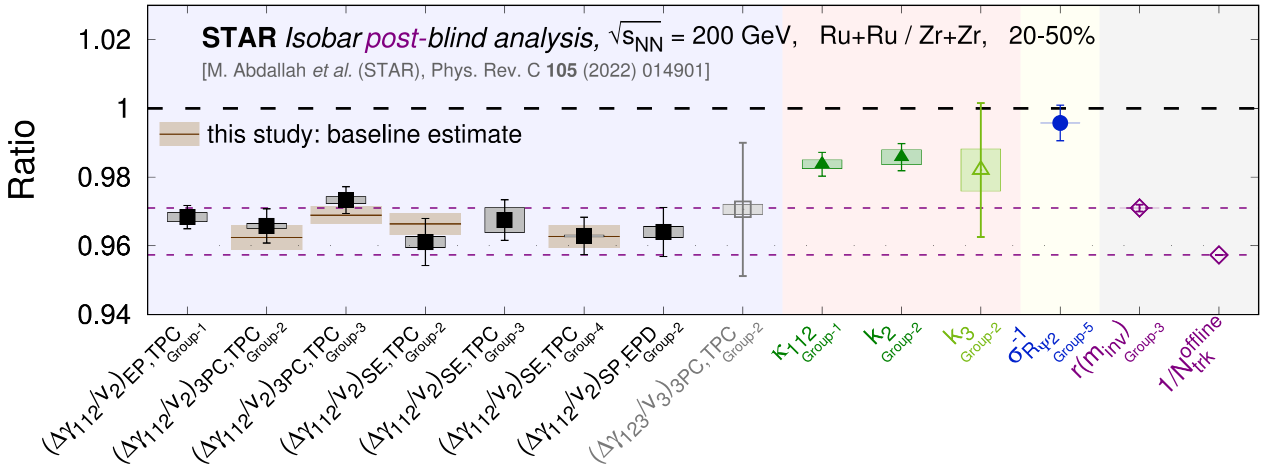

FIG. 3. Isobar measurements of Y from the STAR blind analyses [24], together with background baseline estimates for the four measurements that used the cumulant method.

The average contribution to $Y_{\rm bkgd}$ from 3p correlation backgrounds in 20–50% centrality is around -1.3%.

Results. Figure 2 shows the estimated baseline as a function of centrality, along with the isobar data corresponding to the Group-3 full-event and Group-2 subevent analysis, respectively. The systematic uncertainty on the baseline is taken to be the quadratic sum of the uncertainties on the individual components as described above. Figure 3 depicts the Y measurements in the 20–50% centrality range [24] together with our estimated baselines averaged over the same range. The three terms in the baseline (Eq. (6)) are averaged over centrality individually and then summed. The measured data are consistent with these estimated baselines over most of the centrality bins.

The differences, $Y - Y_{\rm bkgd}$, measure the purported CME signal. The baseline estimates partly come from data. These estimates are derived from quantities and/or methods different from the $\Delta\gamma/v_2$ measurements, so their statistical uncertainties are treated independently. The systematic uncertainties on the isobar measurements were assessed by varying analysis cuts, and were found to be significantly smaller than the statistical uncertainties [24]. We did not repeat those in the baseline calculation ($Y_{\rm bkgd}$) to avoid double counting in systematics, but instead propagate data systematic uncertainties to differences $Y - Y_{\rm bkgd}$ in quadrature.

Our results indicate that the CME signal difference in isobar collisions is consistent with zero within uncertainties. We therefore estimate the upper limit of the possible CME signals. The isobar difference in the magnetic field strengths makes it possible to extract CME signal by comparing the isobar collision systems. Assuming it results in a 15% difference in the CME $\Delta\gamma$ signal [39–41],

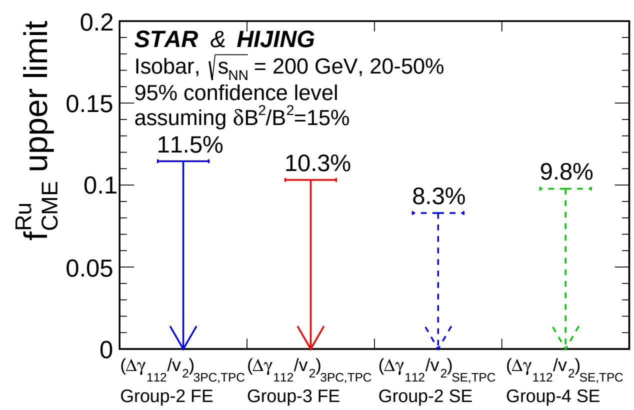

FIG. 4. The $f_{\rm CME}$ upper limits at 95% confidence level from Ru+Ru collisions for the four results in Fig. 3.

then our results translate into an accuracy of a few percent on the CME signal fraction ($f_{\rm CME}$) [31]. We extract an upper limit of $f_{\rm CME} \sim 10\%$ at 95% confidence level [42] for Ru+Ru collisions (Zr+Zr is similar). Figure 4 depicts those upper limits for the four results shown in Fig. 3.

Summary. We reexamine the isobar ratio $Y \equiv \frac{(\Delta\gamma/v_2)^{\rm Ru}}{(\Delta\gamma/v_2)^{\rm Zr}}$, which measures the charge separation due to the chiral magnetic effect (CME) in isobar collisions, and account for the background effects from multiplicity and nonflow correlations. We estimate the background baseline for Y by using 2p and 3p correlations from STAR isobar data and HIJING simulations. The estimated baselines agree with the STAR measurements [24]. We set an upper limit at the 95% confidence level on the CME fraction of $\sim 10\%$ in isobar collisions at $\sqrt{s_{\rm NN}} = 200$ GeV at

RHIC. This study provides interpretations to the previous STAR isobar measurements, and develops a workflow to estimate backgrounds in other and future related CME searches.

ACKNOWLEDGMENTS

We thank the RHIC Operations Group and RCF at BNL, the NERSC Center at LBNL, and the Open Science Grid consortium for providing resources and support. This work was supported in part by the Office of Nuclear Physics within the U.S. DOE Office of Science, the U.S. National Science Foundation, National Natural Science Foundation of China, Chinese Academy of Science, the Ministry of Science and Technology of China and the Chinese Ministry of Education, the Higher Education Sprout Project by Ministry of Education at NCKU, the National Research Foundation of Korea, Czech Science Foundation and Ministry of Education, Youth and Sports of the Czech Republic, Hungarian National Research, Development and Innovation Office, New National Excellency Programme of the Hungarian Ministry of Human Capacities, Department of Atomic Energy and Department of Science and Technology of the Government of India, the National Science Centre and WUT ID-UB of Poland, the Ministry of Science, Education and Sports of the Republic of Croatia, German Bundesministerium für Bildung, Wissenschaft, Forschung and Technologie (BMBF), Helmholtz Association, Ministry of Education, Culture, Sports, Science, and Technology (MEXT) and Japan Society for the Promotion of Science (JSPS).

[1] K. Fukushima, D. E. Kharzeev, and H. J. Warringa, The chiral magnetic effect, Phys.Rev. **D78**, 074033 (2008), arXiv:0808.3382 [hep-ph].

[2] P. D. Morley and I. A. Schmidt, Strong P, CP, T violations in heavy ion collisions, Z. Phys. **C26**, 627 (1985).

[3] D. Kharzeev, R. Pisarski, and M. H. Tytgat, Possibility of spontaneous parity violation in hot QCD, Phys.Rev.Lett. **81**, 512 (1998), arXiv:hep-ph/9804221 [hep-ph].

[4] D. Kharzeev, Parity violation in hot QCD: Why it can happen, and how to look for it, Phys.Lett. **B633**, 260 (2006), arXiv:hep-ph/0406125 [hep-ph].

[5] D. E. Kharzeev, L. D. McLerran, and H. J. Warringa, The Effects of topological charge change in heavy ion collisions: 'Event by event P and CP violation', Nucl.Phys. **A803**, 227 (2008), arXiv:0711.0950 [hep-ph].

[6] M. Dine and A. Kusenko, Origin of the matter-antimatter asymmetry, Rev. Mod. Phys. **76**, 1 (2003).

[7] S. A. Voloshin, Parity violation in hot QCD: How to detect it, Phys.Rev. **C70**, 057901 (2004), arXiv:hep-ph/0406311 [hep-ph].

[8] F. Wang, Effects of Cluster Particle Correlations on Local Parity Violation Observables, Phys.Rev. **C81**, 064902 (2010), arXiv:0911.1482 [nucl-ex].

[9] A. Bzdak, V. Koch, and J. Liao, Remarks on possible local parity violation in heavy ion collisions, Phys.Rev. **C81**, 031901 (2010), arXiv:0912.5050 [nucl-th].

[10] S. Schlichting and S. Pratt, Charge conservation at energies available at the BNL Relativistic Heavy Ion Collider and contributions to local parity violation observables, Phys.Rev. **C83**, 014913 (2011), arXiv:1009.4283 [nucl-th].

[11] B. Abelev *et al.* (STAR Collaboration), Azimuthal Charged-Particle Correlations and Possible Local Strong Parity Violation, Phys.Rev.Lett. **103**, 251601 (2009), arXiv:0909.1739 [nucl-ex].

[12] B. Abelev *et al.* (STAR Collaboration), Observation of charge-dependent azimuthal correlations and possible local strong parity violation in heavy ion collisions, Phys.Rev. **C81**, 054908 (2010), arXiv:0909.1717 [nucl-ex].

[13] B. Abelev *et al.* (ALICE), Charge separation relative to the reaction plane in Pb-Pb collisions at $\sqrt{s_{NN}}$= 2.76 TeV, Phys.Rev.Lett. **110**, 012301 (2013), arXiv:1207.0900 [nucl-ex].

[14] L. Adamczyk *et al.* (STAR), Fluctuations of charge separation perpendicular to the event plane and local parity violation in $\sqrt{s_{NN}}$=200 GeV Au+Au collisions at the BNL Relativistic Heavy Ion Collider, Phys. Rev. **C88**, 064911 (2013), arXiv:1302.3802 [nucl-ex].

[15] L. Adamczyk *et al.* (STAR), Measurement of charge multiplicity asymmetry correlations in high-energy nucleus-nucleus collisions at $\sqrt{s_{NN}} = 200$ GeV, Phys. Rev. **C89**, 044908 (2014), arXiv:1303.0901 [nucl-ex].

[16] L. Adamczyk *et al.* (STAR), Beam-energy dependence of charge separation along the magnetic field in Au+Au collisions at RHIC, Phys. Rev. Lett. **113**, 052302 (2014), arXiv:1404.1433 [nucl-ex].

[17] J. Adam *et al.* (STAR), Charge-dependent pair correlations relative to a third particle in p + Au and d+ Au collisions at RHIC, Phys. Lett. **B798**, 134975 (2019), arXiv:1906.03373 [nucl-ex].

[18] M. S. Abdallah *et al.* (STAR), Pair invariant mass to isolate background in the search for the chiral magnetic effect in Au + Au collisions at sNN=200 GeV, Phys. Rev. C **106**, 034908 (2022), arXiv:2006.05035 [nucl-ex].

[19] M. Abdallah *et al.* (STAR), Search for the Chiral Magnetic Effect via Charge-Dependent Azimuthal Correlations Relative to Spectator and Participant Planes in Au+Au Collisions at $\sqrt{s_{NN}} = 200$ GeV, Phys. Rev. Lett. **128**, 092301 (2022), arXiv:2106.09243 [nucl-ex].

[20] V. Khachatryan *et al.* (CMS), Observation of charge-dependent azimuthal correlations in p-Pb collisions and its implication for the search for the chiral magnetic effect, Phys. Rev. Lett. **118**, 122301 (2017), arXiv:1610.00263 [nucl-ex].

[21] A. M. Sirunyan *et al.* (CMS), Constraints on the chiral magnetic effect using charge-dependent azimuthal correlations in pPb and PbPb collisions at the CERN Large Hadron Collider, Phys. Rev. **C97**, 044912 (2018), arXiv:1708.01602 [nucl-ex].

[22] S. Acharya *et al.* (ALICE), Constraining the magnitude of the Chiral Magnetic Effect with Event Shape Engineering in Pb-Pb collisions at $\sqrt{s_{\rm NN}} = 2.76$ TeV, Phys. Lett. **B777**, 151 (2018), arXiv:1709.04723 [nucl-ex].

[23] S. Acharya *et al.* (ALICE), Constraining the Chiral Magnetic Effect with charge-dependent azimuthal correlations in Pb-Pb collisions at $\sqrt{s_{\rm NN}} = 2.76$ and 5.02 TeV,

JHEP **09**, 160, arXiv:2005.14640 [nucl-ex].

[24] M. Abdallah *et al.* (STAR), Search for the chiral magnetic effect with isobar collisions at $\sqrt{s_{NN}}$=200 GeV by the STAR Collaboration at the BNL Relativistic Heavy Ion Collider, Phys. Rev. C **105**, 014901 (2022), arXiv:2109.00131 [nucl-ex].

[25] S. A. Voloshin, Testing the chiral magnetic effect with central U+U collisions, Phys.Rev.Lett. **105**, 172301 (2010), arXiv:1006.1020 [nucl-th].

[26] V. Koch, S. Schlichting, V. Skokov, P. Sorensen, J. Thomas, S. Voloshin, G. Wang, and H.-U. Yee, Status of the chiral magnetic effect and collisions of isobars, Chin. Phys. **C41**, 072001 (2017), arXiv:1608.00982 [nucl-th].

[27] H.-J. Xu, X. Wang, H. Li, J. Zhao, Z.-W. Lin, C. Shen, and F. Wang, Importance of isobar density distributions on the chiral magnetic effect search, Phys. Rev. Lett. **121**, 022301 (2018), arXiv:1710.03086 [nucl-th].

[28] H. Li, H.-j. Xu, J. Zhao, Z.-W. Lin, H. Zhang, X. Wang, C. Shen, and F. Wang, Multiphase transport model predictions of isobaric collisions with nuclear structure from density functional theory, Phys. Rev. **C98**, 054907 (2018), arXiv:1808.06711 [nucl-th].

[29] H.-j. Xu, H. Li, X. Wang, C. Shen, and F. Wang, Determine the neutron skin type by relativistic isobaric collisions, Phys. Lett. B **819**, 136453 (2021), arXiv:2103.05595 [nucl-th].

[30] D. E. Kharzeev, J. Liao, and S. Shi, Implications of the isobar-run results for the chiral magnetic effect in heavy-ion collisions, Phys. Rev. C **106**, L051903 (2022), arXiv:2205.00120 [nucl-th].

[31] M. Abdallah *et al.* (STAR), Estimate of Background Baseline and Upper Limit on the Chiral Magnetic Effect in Isobar Collisions at $\sqrt{s_{\rm NN}}$ = 200 GeV at the Relativistic Heavy-Ion Collider, (2023), to be published in Phys. Rev. C, arXiv:2310.13096 [nucl-ex].

[32] J.-Y. Ollitrault, Anisotropy as a signature of transverse collective flow, Phys.Rev. **D46**, 229 (1992).

[33] A. M. Poskanzer and S. Voloshin, Methods for analyzing anisotropic flow in relativistic nuclear collisions, Phys.Rev. **C58**, 1671 (1998), arXiv:nucl-ex/9805001 [nucl-ex].

[34] Y. Feng, J. Zhao, H. Li, H.-j. Xu, and F. Wang, Two- and three-particle nonflow contributions to the chiral magnetic effect measurement by spectator and participant planes in relativistic heavy ion collisions, Phys. Rev. C **105**, 024913 (2022), arXiv:2106.15595 [nucl-ex].

[35] D. Shen, J. Chen, A. Tang, and G. Wang, Impact of globally spin-aligned vector mesons on the search for the chiral magnetic effect in heavy-ion collisions, Phys. Lett. B **839**, 137777 (2023), arXiv:2212.03056 [nucl-th].

[36] G. Yan, Probing Initial- and Final-state Effects of Heavy-ion Collisions with STAR Experiment, *Proceedings, 29th International Conference on Ultrarelativistic Nucleus-Nucleus Collisions (Quark Matter 2022): Krakow, Poland, April 4-10, 2022*, Acta Phys. Pol. B Proc. Suppl. **16-1-A**, 137 (2023).

[37] X.-N. Wang and M. Gyulassy, HIJING: A Monte Carlo model for multiple jet production in p p, p A and A A collisions, Phys.Rev. **D44**, 3501 (1991).

[38] M. Gyulassy and X.-N. Wang, HIJING 1.0: A Monte Carlo program for parton and particle production in high-energy hadronic and nuclear collisions, Comput.Phys.Commun. **83**, 307 (1994), arXiv:nucl-th/9502021 [nucl-th].

[39] V. Skokov, A. Yu. Illarionov, and V. Toneev, Estimate of the magnetic field strength in heavy-ion collisions, Int. J. Mod. Phys. **A24**, 5925 (2009), arXiv:0907.1396 [nucl-th].

[40] A. Bzdak and V. Skokov, Event-by-event fluctuations of magnetic and electric fields in heavy ion collisions, Phys. Lett. **B710**, 171 (2012), arXiv:1111.1949 [hep-ph].

[41] W.-T. Deng and X.-G. Huang, Event-by-event generation of electromagnetic fields in heavy-ion collisions, Phys. Rev. **C85**, 044907 (2012), arXiv:1201.5108 [nucl-th].

[42] G. J. Feldman and R. D. Cousins, A Unified approach to the classical statistical analysis of small signals, Phys. Rev. **D57**, 3873 (1998), arXiv:physics/9711021 [physics.data-an].